

Summary

12/12/14, 1:20:21 PM

Differences exist between documents.

New Document:

[CT_Pipeline_Template_rewrite_2014Nov18](#)

34 pages (4.37 MB)

12/12/14, 1:19:40 PM

Used to display results.

Old Document:

[CT_Pipeline_Template_rewrite_2014Aug12](#)

27 pages (3.80 MB)

12/12/14, 1:19:38 PM

[Get started: first change is on page 2.](#)

No pages were deleted

How to read this report

Highlight indicates a change.

Deleted indicates deleted content.

 indicates pages were changed.

 indicates pages were moved.

All authors have read and approved the submitted manuscript, the manuscript has not been submitted elsewhere nor published elsewhere in whole or in part.

Title Page

Quantitative Localization and Predictive Performance of **Supratentorial** Intracranial Hemorrhage

John Muschelli^{1,*}, ScM; Natalie L. Ullman², BS; Elizabeth M. Sweeney¹, ScM; Ani Eloyan¹, PhD; Neil Martin³, MD; Paul Vespa³, MD; Daniel F. Hanley², MD; Ciprian M. Crainiceanu¹, PhD

1 Department of Biostatistics, Bloomberg School of Public Health, Johns Hopkins University, Baltimore, MD

2 Department of Neurology, Division of Brain Injury Outcomes, Johns Hopkins Medical Institutions, Baltimore, MD

3 Department of Neurosurgery, David Geffen School of Medicine at UCLA, Los Angeles, CA

4 Section of Neurosurgery and the Neurovascular Surgery Program, University of Chicago Pritzker School of Medicine, Chicago, IL

* **E-mail:** jmusche1@jhu.edu

Abstract

Background and Purpose

Current studies of association between intracranial hemorrhage (ICH) localization and stroke severity present conflicting evidence. Using advanced registration techniques on computed tomography (CT) brain scans, we provide detailed quantification of ICH location and its association with stroke outcomes.

Methods

We analyzed 111 scans from 111 patients enrolled in the MISTIE (Minimally Invasive Surgery plus recombinant-tissue plasminogen activator for Intracerebral Evacuation) trial. We registered CT scans to a CT template, estimated a 3-dimensional map of ICH engagement location, and derived regions predictive of 2 severity scores: the National Institutes of Health Stroke Scale (NIHSS) and Glasgow Coma Scale (GCS) scores. We compared the prediction performance of these regions compared to using location information determined by human readers by means of the adjusted R^2 from linear regression models and tested differences between models using a permutation test.

Results

In this sample, ICH primarily located in deep brain nuclei and lobar white matter, including the superior corona radiata and the thalamus, is related to severity scores. The patient severity predictive performance was twice as good for the image-based model compared to the reader-based model (adjusted R^2 : 0.254 vs. 0.129 for NIHSS, 0.214 vs. 0.069 for GCS, all $p < .01$, uncorrected).

Conclusions

Measures of ICH location and engagement using advanced CT imaging processing provide finer, more quantitative, and more predictive anatomic information than that provided by expert human readers. These findings suggest that important anatomic relationships may play biologically plausible roles in determining the severity of a particular ICH and can be estimated using this analytic platform.

Clinical Trial Registration Information

Clinical Trial Registration-URL: <http://www.clinicaltrials.gov>. Unique identifier: NCT00224770.

Keywords: Intracerebral Hemorrhage; CT and MRI; severity score prediction

Introduction

The clinically determined stroke location is not a robust predictor of severity or outcome in either ischemic stroke [1] or intracranial hemorrhage (ICH) [2]. This is particularly true for ICH, which results from a blood vessel rupturing into brain tissues and possibly the ventricles where bleeding causes distension and sometimes destruction of brain structures.

For patients with ICH, X-ray computed tomography (CT) scanning is used because it is widely available and is highly sensitive to the presence of blood [3]. Clinicians utilize CT to define the location of bleeding, clinically assess severity, and plan patient management. Despite the clinical focus on site of bleeding, other measures of injury (ICH volume, NIHSS, and age), but not location, are the main predictors of severity and outcome. Early attempts to use location in the well-defined Stroke Data Bank population found no influence for the anatomic location of ICH in predictions [2]. Subsequent convenience samples have reaffirmed the importance of brainstem injury as a factor in predicting outcome [4], but have not demonstrated any influence of different supratentorial locations [2, 4-9]. Importantly, clinical trials have not found location to be a critical factor associated with beneficial clinical outcome [10-13]. Thus, we decided to investigate the combination of location and volume to determine if quantitative location information might better inform our understanding of tissue injury in ICH. We have tested a productive strategy from ischemic stroke and MRI research [14] utilizing the anatomic data from CT.

Problems with Visual Inspection

The classification of hemorrhage location is complicated for even the best-trained neuroimaging scientists. For example, a hemorrhage may extend into multiple brain areas, distend tissues altering anatomic relationships, and may break through the ventricular wall. Evaluating these anatomic possibilities challenges even the best clinicians, thus routine practice identifies a single location as the primary affected anatomic region (e.g. caudate, putamen, etc.) or describes the location of the edge of the hemorrhage in relation to a given landmark [15]. Outcome is strongly associated with hemorrhage volume; importantly, the modulation of the relationship between volume and location has not been studied.

Previous CT Registration Work

To investigate these anatomic issues, detailed localization information can be obtained by registering scans to a common template to provide refined anatomical localization information. Registration to template space is a crucial first step for any across-patient analysis; this allows each patient's scan to be located in the same stereotaxic space so information may be combined spatially across scans. Moreover, brain atlases with spatially defined anatomic structures are available in template space. Recently, Rorden et al. [16]

released the first publicly available CT template of healthy adults in MNI (Montreal Neurological Institute) space. This template image allows for a straightforward registration where the reference and template images are in a single imaging modality as opposed to more complex referencing systems [17-19].

Hypothesis

We propose to use CT images from the MISTIE (Minimally Invasive Surgery plus recombinant tissue plasminogen activator for Intracerebral Evacuation) trial to investigate the benefit or lack thereof in utilizing anatomic location as a biologically plausible predictor of ICH severity. Thus, we propose to test the hypothesis that routine clinical anatomic localization was no different than quantitative localization derived from registered-to-template images with atlas-based labeling for prediction of severity of injury.

Methods

To address this hypothesis, we will 1) create a 3-dimensional (3D) density map of hemorrhages occurring in a population of patients with ICH; 2) provide detailed quantification of hemorrhage engagement of individual neuroanatomic regions within the brain; 3) determine if differences in location relate to initial patient severity as described by two common disability scores: the National Institutes of Health Stroke Scale (NIHSS) [20] and the modified Glasgow Coma Scale (GCS) [21, 22]; and 4) generate a stroke region of engagement that is likely to be associated with stroke severity as well as test its predictive performance using within-sample validation.

Subjects and Demographics

The population studied consists of 111 patients from MISTIE recruited from 26 centers with lobar and deep ICHs ≥ 20 cc in volume [23]. CT and clinical data were collected as part of the Johns Hopkins Medicine IRB-approved MISTIE research studies with written consent from participants.

The NIHSS and GCS scores were recorded at enrollment; 3 patients did not have a recorded NIHSS score, 1 patient did not have a recorded GCS score. These patients were excluded from the analyses associating NIHSS and GCS scores and location, respectively. All patients were included in the construction of the 3D histogram image.

Descriptive demographics of age, sex, race, baseline ICH and intraventricular hemorrhage (IVH) volume, and NIHSS and GCS scores are shown in Table 1. The NIHSS score reflects stroke-related impairment (higher is worse), while the GCS score reflects a patient's level of consciousness (higher is better).

Imaging Data

Standard diagnostic CT images of the MISTIE trial subjects were registered to template space. The study protocol was executed with minor, but important, differences across the 26 sites. Scans were acquired using GE ($N=46$), Siemens ($N=37$), Philips ($N=20$), and Toshiba ($N=8$) scanners. Gantry tilt was observed in 87 scans. Slice thickness of the image varied within the scan for 14 scans, referred to as variable slice thickness. For example, a scan may have 10 millimeter (mm) slices at the top and bottom of the brain, where no ICH is present, but with 5mm slices in the middle where the ICH is seen (see <http://stroke.ahajournals.org>). Therefore, the scans analyzed had different voxel (volume element) dimensions and image resolution prior to registration to the template. These conditions represent a pragmatic sample of stroke center diagnostic imaging.

Hemorrhage Segmentation and Location Identification

ICH was manually segmented on CT scans using the OsiriX imaging software by expert readers (v.4.1, Pixmeo; Geneva, Switzerland). Readers employed a semi-automated threshold-based approach: a Hounsfield unit (HU) range of 40 to 80 selected potential regions of ICH [24, 25], then these regions were refined by including or excluding regions using manual adjustment of ICH. Readers also identified the specific anatomic location most engaged by the ICH (Table 1).

Image Registration

The DICOM (Digital Imaging and Communications in Medicine) data was preprocessed to obtain a 3D brain image (see <http://stroke.ahajournals.org> for details). The image was then spatially registered to the CT template using the Clinical toolbox [16], which employs the unified normalization-segmentation routine [26] from the statistical parametric mapping software (version 8, SPM8, Wellcome Trust Centre for Neuroimaging, London, UK) in MATLAB (The Mathworks, Natick, Massachusetts, USA). The binary hemorrhage mask was transformed into the template space. No scans were excluded due to inadequate registration, determined by visual inspection by expert CT readers.

Histograms of ICH in the Brain

All subsequent statistical analysis and data manipulation was done in the R statistical programming language (<http://cran.r-project.org/>). To visualize and describe the localization of ICH, we first combined information from registered masks of 111 patients. Using these ICH masks, we obtained the 3-dimensional (3D) histogram of ICH localization for the study population. More precisely, for every voxel in the template space, we calculated the proportion of patients who have an ICH at that particular voxel. We

I used the `brainR` package to create an 3D interactive map of the 3D histogram [27] (http://muscchellij2.github.io/CT_Pipeline/index.html).

ICH Localization and Engagement

We calculated spatial ICH engagement by neuroanatomic region using the “Eve” atlas [28], which segments gray matter (GM) and white matter (WM) regions. Ventricular regions were not explicitly segmented; any region not classified as GM or WM were classified as cerebrospinal fluid (CSF).

From this atlas, we estimated for each patient scan: 1) the percent of the ICH engaged by region (e.g. putamen engages 20% of the ICH) and 2) the percent of each region engaged by the ICH (e.g. ICH engages 78% of the putamen). These summaries of ICH engagement provide a much finer description of location than what can currently be done by expert human readers (e.g. putaminal bleed).

We further summarized neuroanatomic engagement at the population level (see <http://stroke.ahajournals.org> for details).

Prediction of Severity Score Based on Hemorrhage Location

In the study population, 1,045,174 voxels (denoted by V) had at least one patient with ICH. We limited our analysis to voxels in the template space where at least 10 patients exhibit ICH (166,202 voxels) to optimize the models for a substantial proportion of the study population.

We tested the association between hemorrhage location and stroke severity (NIHSS or GCS score) by running a series of models, accounting for confounders. At each voxel, we ran a linear regression model:

$$Y_i = \beta_0 + \beta_1(v)ICH_i(v) + \gamma X_i + \epsilon_i(v), \quad (1)$$

where Y_i was either the NIHSS or GCS score for patient $i=1, \dots, 111$, $ICH_i(v)$ is a binary indicator where $ICH_i(v)=1$ if patient i 's ICH mask has a 1 at voxel v , and $ICH_i(v)=0$ otherwise. X_i is a vector of patient-specific confounders with effects γ and $\epsilon_i(v)$ are assumed independent homoscedastic errors. The confounders, X_i , either were excluded for “unadjusted” voxel-level model, or contains a combination of 3 patient-specific confounders: age, sex, and total baseline ICH volume (TotalVol) in the “adjusted” models. We used the unadjusted Wilcoxon rank-sum test on Y at every voxel to confirm that results are robust to the choice of test statistic.

P-values of each voxel-wise model were calculated, testing the null hypothesis $H_0(v)$: $\beta_1(v)=0$, or in the case of the Wilcoxon rank-sum test: $H_0(v):Severity\{ICH(v)=1\}=Severity\{ICH(v)=0\}$ where $Severity$ denotes the distribution of severity scores of patients. We investigated whether individual locations are predictive of severity score after

accounting for multiple comparisons using a Bonferroni correction with a family wise error rate of $\alpha=.05$.

Highest Predictive Region Generation and Analysis

In order to create a patient-level covariate that summarizes ICH location information, we selected regions based on uncorrected voxel-wise p-values from the unadjusted linear model using a sequence of nested thresholds. We call these regions “highest predictive regions” (HPR) because they contain the voxels that are most predictive of the severity scores. We obtained 6 different HPR, 3 based on the smallest 1000, 2000, or 3000 lowest p-values and three based on p-values thresholds of .05, .01, and .001. For each HPR, we calculated the HPR “coverage”— the percentage of the voxels in the HPR that were classified as hemorrhage in the subject-specific image:

$$\text{HPR Coverage}_i = \frac{\# \text{ Voxels classified ICH in HPR for scan } i}{\# \text{ Voxels in HPR}} \times 100\%$$

If a patient’s ICH covers the entire HPR, the coverage is 100%, whereas if no overlap exists between the patient’s ICH and HPR then coverage is 0%. The HPR coverage is then used as a predictor of the severity score in the adjusted model:

$$Y_i = \beta_0 + \beta_1 \text{Coverage}_i + \gamma_1 \text{Age}_i + \gamma_2 \text{Sex}_i + \gamma_3 \text{TotalVol}_i + \epsilon_i \quad (2)$$

We compared model (2) to one using a categorical indicator of the expert-specified ICH location, with categories: thalamus, globus pallidus, putamen, and lobar. Prediction performance and model fit were assessed using R^2 , adjusted R^2 , Akaike information criterion (AIC) [29], and root mean squared error (RMSE).

We have also tested the null hypothesis that the prediction performance of the obtained HPRs was consistent with the prediction performance of the HPRs obtained using the same procedure when there is no association between stroke severity scores and location. A permutation test was used where the severity score was randomly permuted, the method for obtaining the HPR was applied to the data with permuted severity scores, and the adjusted R^2 was calculated for each such permutation. The p-value was obtained by comparing the permutation distribution of the adjusted R^2 with the adjusted R^2 obtained from the original data. This was necessary to address both the testing multiplicity problem and the double use of the outcome variable when selecting the HPR.

In addition, we have performed 10-fold cross-validation of the results. That is, we have split the data in training and test using a 90%/10% split (10% for test). For each such split we have created the HPR and the HPR coverage, and fit the adjusted models with the HPR coverage and reader-based location separately. On the 10% test sample, we have calculated the HPR percentage and predicted the NIHSS or GCS for those patients from these adjusted models. We repeated this step 10 times for each of the 10 test data

sets. We calculated the mean squared error (MSE) by the formula $\frac{1}{n} \sum_{i=1}^n (Y_i - \hat{Y}_i)^2$ for the location model and for each p-value threshold, where Y_i and \hat{Y}_i denote the outcome and predicted outcome, respectively, for patient i . The cross-validated MSE was computed for each HPR coverage model and the reader-based location model. For comparison of model performance this MSE is less prone to overfitting from using the outcome variable in both HPR generation and model estimation.

Results

Prevalence of ICH Engagement in the Brain

The distribution of the prevalence of ICH over all voxels shows the majority of voxels have a low prevalence of ICH engagement; the median number of patients with ICH at a given voxel is 3 (3%), though a small group of voxels ($V=5685$) have a high prevalence of >40% of the sample population. Figure 1 represents the 3D histogram of hemorrhage prevalence, where colors represent the percentage of patients with ICH engagement at that given area. This image indicates that ICH is distributed medially in the brain in this cohort, with a lower concentration at the cortical surface and higher on the left side of the brain. Figure 1 also indicates that the prevalence of strokes in the extreme anterior and posterior areas of the brain is very low.

Prediction of Functional Score Based on Hemorrhage Location

To study the association between localization and stroke severity scores, we have fit model (1) using a sequence of potential confounding adjustments. More precisely, the five voxel-wise linear models fit were:

$$\begin{aligned}\mathcal{M}_1 : \quad Y_i &= \beta_0 + \beta_1(v)\text{ICH}_i(v) + \epsilon_i(v), \\ \mathcal{M}_2 : \quad Y_i &= \beta_0 + \beta_1(v)\text{ICH}_i(v) + \gamma_1(v)\text{Age}_i + \epsilon_i(v), \\ \mathcal{M}_3 : \quad Y_i &= \beta_0 + \beta_1(v)\text{ICH}_i(v) + \gamma_2(v)\text{Sex}_i + \epsilon_i(v), \\ \mathcal{M}_4 : \quad Y_i &= \beta_0 + \beta_1(v)\text{ICH}_i(v) + \gamma_3(v)\text{TotalVol}_i + \epsilon_i(v), \\ \mathcal{M}_5 : \quad Y_i &= \beta_0 + \beta_1(v)\text{ICH}_i(v) + \gamma_1(v)\text{Age}_i + \gamma_2(v)\text{Sex}_i + \gamma_3(v)\text{TotalVol}_i + \epsilon_i(v),\end{aligned}$$

where \mathcal{M} denotes a model. For consistency of notation (as it is not an explicit model) we refer to the Wilcoxon rank-sum test as \mathcal{M}_6 . Figure 2 displays the voxel-wise p-values from NIHSS score models, overlaid on a T1 magnetic resonance image (MRI) for spatial localization of structures (\mathcal{M}_3 and \mathcal{M}_4 are not shown, and appear similar to Figure 2C, see <http://stroke.ahajournals.org> for GCS models). The p-value images displayed were not corrected since the purpose is to investigate regional brain anatomy where ICH engagement could relate to severity score.

The estimated association of location and NIHSS can be visualized by comparing the location of high and low p-values. Figure 2 indicates the strongest associations are clustered in the immediate vicinity of the medial plane both for the GCS (see <http://stroke.ahajournals.org>) and NIHSS scores. The p-values are higher (more blue) in the models adjusted for age (not shown), baseline ICH volume (not shown), and both age and baseline ICH volume (Figure 2C) compared to the unadjusted model \mathcal{M}_1 . This distribution agrees with Figure 2 from Menezes et al. [14], which presents the locations which affect NIHSS in a similar analysis of patients with ischemic stroke using MRI (T2 images).

No voxels were significantly related to NIHSS score or GCS score in any model after using the Bonferroni correction.

Highest Predictive Region Analysis

We investigated whether we can define areas of the brain that can improve prediction of stroke severity scores. The HPR and HPR coverage were calculated. The HPR with the .05, .01, and .001 p-value thresholds, corresponded to HPR with 47,736, 19,047, and 2,422 voxels for NIHSS and 52,368, 22,858, and 4,669 voxels for GCS, respectively. For illustration, panel (A) in Figure 3 displays the region of p-values smaller than .01 in the unadjusted NIHSS regression model, and panel (B) displays the region with the smallest 1000 p-values for the unadjusted regression of GCS score. We show three orthographic slices for each HPR; the entire regions are available in MNI coordinates.

While the voxel-wise p-values identify areas that are potentially highly associated with the outcome, we want to reduce these complex HPR to a simple subject-specific covariate, HPR coverage. Figure 3C displays the NIHSS score as a function of the coverage of the HPR from Figure 3A. Similarly, Figure 3D displays the GCS score as a function of the coverage of the HPR in Figure 3B. The blue line represents a non-parametric LOESS (local regression) fit and the red line represents an unadjusted linear model fit. As expected, the larger the HPR coverage the higher (more severe stroke) the NIHSS score and the lower (deeper unconsciousness) the GCS score.

Combining regions of engagement from the left and right sides of the brain is worthwhile as regions will likely affect severity regardless of the hemisphere engaged. We did not combine these areas, as it may not be straightforward to combine ICH that crosses the mid-sagittal plane. We did attempt to “symmetrize” the HPR by including voxels regardless of the side of the brain. If a voxel on the left side of the brain was included in the HPR, the corresponding voxel on the right side was included in the symmetrized HPR. We observed similar patterns to Figure 3C and 3D using the symmetrized HPR (see <http://stroke.ahajournals.org>).

We further investigated how these regions predict severity compared to ICH location classification provided by expert readers. Table 2 compares prediction performance based on the expert readers' location (labeled “Location model”) versus using HPR coverage

for NIHSS and GCS scores. Adjusted R^2 model estimates indicated all HPR coverage models strongly outperform reader-classified location models. Indeed, for NIHSS, the adjusted R^2 almost doubled from 0.129 for the reader-classified location model to 0.254 for the best HPR coverage model. For GCS, the adjusted R^2 more than tripled from 0.069 for the reader-classified location model to 0.214 for the HPR coverage model. We concluded that all HPR coverage models strongly outperform reader-classified location models, regardless of using adjusted R^2 , R^2 , AIC, or RMSE as criteria. The other HPR coverage models provide relatively comparable prediction performance. This indicates that the choice of one HPR versus another may need to be based on other criteria, such as total HPR volume, ICH population prevalence, and prior biological information. Please see <http://stroke.ahajournals.org> for a table of coefficients for the best HPR and location models.

The permutation test p-values were $< .001$ for HPR of NIHSS and $< .01$ for HPR of GCS, indicating that the selected HPRs were more predictive than HPRs obtained using the same selection procedure when there is no association between location and stroke severity scores.

For the cross-validated analysis, the model with the lowest MSE was the one containing the coverage from the HPR with a p-value threshold of 0.05 for GCS (MSE = 8.20), and the HPR coverage from the top 3000 p-values for NIHSS (MSE = 65.16). Models using the reader-assessed location had higher (i.e. worse) MSE (GCS: 9.09, NIHSS: 72.9) than all models containing the HPRs for both outcomes, except for the HPR for NIHSS using a p-value threshold of 0.001 (MSE = 79.4).

ICH Localization and Engagement

Table 3 represents the 10 most-engaged regions for the population 3D histogram as well as the best-performing HPR from the GCS and NIHSS score analyses. The engagement represents the percent engagement of a specific area compared to all areas engaged. The 3D histogram of ICH is engaged in areas of the insular, putamen, and primarily the CSF, such as the ventricles.

The HPR based on the NIHSS analysis engages primarily areas of the internal capsule, thalamus, superior corona radiata, and CSF regions. Venkatasubramanian et al. [30] found that Wallerian degeneration [31] in the corticospinal tract (CST) was related worse NIHSS. Jang et al. [32] demonstrated that those with intact CST had better outcomes on the motricity index of upper extremity (UMI) [33] and Modified Brunnstrom classification (MBC) [34], which would indicate that many similar motor functions captured by the NIHSS would be affected. Schaechter et al. [35] found, using diffusion tensor imaging that decreased fractional anisotropy (FA) in the precentral gyrus, superior and anterior corona radiata and orbitofrontal region correlated to a poorer motor outcome in patients with ischemic stroke.

The HPR based on the GCS analysis engages primarily the thalamus and superior

corona radiata. In a study with only hemorrhagic bleeds in the thalamus, Kumral et al. [36] found GCS related to thalamic hemorrhage volume. Therefore, we have found areas previously related to each outcome. One limitation of using the NIHSS and GCS as outcomes is that many analyses of location are based on motor scores such as the Medical Research Council (MRC) scale, , other functional outcomes rather than stroke severity scores.

ICH can cause a break in the ventricular wall and intraventricular hemorrhages (IVH) may be present as specified in our inclusion criteria. Though these areas do not represent areas of tissue that can affect severity, they may indicate hemorrhage in the ventricular spaces corresponds to worse stroke severity. Additionally, registering images with large deformations caused by the stroke hemorrhage, even using non-linear registration, will likely have mis-registration artifacts in some areas of the brain. One potential problem is the lateral shift caused by the hemorrhage, which can result in the compression of ventricles. This compression may lead to mapping some areas of the hemorrhage or tissue to the ventricles of the template space. Moreover, one limitation of using the Eve atlas, or any other atlas, is that not every voxel may not be labeled with a corresponding anatomic area. Namely, areas of the ventricular space were not labeled. Other, small areas, such as regions of subarachnoid space, were not labeled either and were included in the CSF region. Therefore, template-space ICH masks may overlap with areas labeled CSF.

To investigate to what extent IVH influences the results, we conducted an additional analysis on subjects with no IVH. Specifically, we provide density maps for patients with no IVH, as categorized by manual readers (Supplemental Figure IV). There is a small percentage (under 5% of patients, blue) of CSF voxels in the template that still have hemorrhage categorized, which indicates that mis-registration of the ventricles may still be present.

In addition to the estimated areas of engagement, we calculated the engagement of the thalamus, putamen and globus pallidus by the population 3D histogram and the HPR for the GCS and NIHSS score analyses (see <http://stroke.ahajournals.org>). The population engagement represents the mean proportion of the ICH prevalence in the population for that brain region. The HPR engagement represents the percent of voxels in that brain region (e.g. putamen) that are in the HPR. On average, 23% of the putamen, 20% of the globus pallidus, and 8% of the thalamus are engaged with ICH from patients in this study. The HPR from the NIHSS analysis engages 40% of the globus pallidus, 6% of the putamen, and 9% of the thalamus. The HPR from the GCS analysis engages only 2% of the thalamus, but not the putamen or the globus pallidus; the GCS HPR is small (1000 voxels).

Discussion

Semi-Automated Localization of ICH

We have characterized the localization of ICH in a population from prospective clinical trial images using a 3D histogram. We found the well-described medial location of most ICHs. Interestingly, location appears to have an influence on initial severity independent of other more established severity factors. This influence is plausibly related to the proximity of the ICH to the corona radiata and internal capsule. This objective method of quantitatively defining anatomic location shows promise over the traditional clinical regional assignment.

We can use this process to create a 3D histogram based on different study populations, or subgroups of such populations or mirror clinical trial inclusion criteria in administrative populations where images are available. As the values in the 3D histogram represent proportions, these images can then be used to test differences between the groups using standard proportion tests. This process allows us to directly compare ICH location in 2 groups at a finer scale than currently available.

Moreover, the pipeline described is semi-automated allowing for more reproducible and objective analyses of larger populations. The only non-automated steps in our pipeline are the ICH segmentation and the export of ICH masks from OsiriX.

Estimation of ICH Engagement with Neuroanatomic Regions

Although 3D histogram maps summarize ICH engagement, many clinicians want descriptions of location in terms of known neuroanatomic regions. We demonstrate how a segmented atlas (Eve) can be used to automatically describe ICH engagement by neuroanatomic regions at a patient or population level. These measures are more interpretable for clinical relevance and may translate to better determination of disability.

Voxel-wise Analysis of Severity Scores

The resulting p-values from the voxel-wise hypothesis tests indicate that ICH engagement near the lateral ventricles may be related to severity scores, regardless of adjustment for known severity factors such as age and lesion volume. None of the voxels passed the stringent Bonferroni correction; a large number of voxels were tested. Each voxel is not independent of the other voxels; therefore, this correction is too conservative. Other methods accounting for this dependence may be more powerful at voxel detection. The voxel-wise p-values provided a voxel screening procedure to generate a HPR for patient-level analysis.

Highest Predictive Region Analysis

The tests in the HPR analysis reject our hypothesis that routine clinical anatomic localization was no different than quantitative localization derived from registered-to-template images for prediction of injury severity. Although prediction performance was quite low even for the best HPR models, prediction performance doubled or tripled, depending on the severity score. Moreover, a cross-validated measure of performance also showed demonstrable gains over using the reader-based categories commonly used in analysis.

This analysis focused on NIHSS and GCS scores, as these were available at enrollment; we analyzed data prior to separation induced by the trial intervention. This process may be applied to long-term functional scores, such as the modified Rankin scale [37, 38].

Summary

The summary of Eve-atlas ICH engagement presented provided a much finer description of location than previously possible by expert human readers. We have shown that using image-based measurements better predicts initial severity scores compared to using clinical location. This type of analysis opens a framework for rigorous testing of location and derivation of objective measures of ICH engagement.

Limitations

This set of patients is defined by the MISTIE inclusion criteria and represents a small proportion of the population of patients with ICH. Larger numbers of subjects and a larger range of ICH location would provide a much-improved assessment of the true ICH prevalence and prediction performance of quantitative location measures. Validation of these regions on an independent dataset of ICH patients would strengthen the argument of detecting regions of the brain where ICH is most related to stroke severity. Though an independent dataset would be ideal, to our knowledge, no datasets are publicly available for testing, particularly with digital masks of ICH. Also, the current description of hemorrhages and all subsequent analyses are reliant on one specific registration technique. Trying multiple registration approaches and comparing results across registrations is likely better [39].

One of the limitations with the HPR analysis is the severity score is used twice: once to find voxels most associated with severity and then regressing HPR coverage on severity. The cross-validation was used as an internal validation and we aim to externally validate the results by studying the performance of the HPR on an independent set of MISTIE patients having the same inclusion criteria when such populations become available.

Sources of Funding

The project described was supported by the NIH grant RO1EB012547 from the National Institute of Biomedical Imaging And Bioengineering, T32AG000247 from the National Institute on Aging, R01NS046309, RO1NS060910, RO1NS085211, R01NS046309, U01NS080824 and U01NS062851 from the National Institute of Neurological Disorders and Stroke, and RO1MH095836 from the National Institute of Mental Health.

Disclosures

Johns Hopkins University holds a use patent for intraventricular tissue plasminogen activator.

References

- [1] Saver, JL, Johnston, KC, Homer, D, Wityk, R, Koroshetz, W, Truskowski, LL, et al. Infarct volume as a surrogate or auxiliary outcome measure in ischemic stroke clinical trials. *Stroke*. 1999;30:293–298.
- [2] Tuhrim, S, Horowitz, DR, Sacher, M, and Godbold, JH. Validation and comparison of models predicting survival following intracerebral hemorrhage. *Critical care medicine*. 1995;23:950–954.
- [3] Sahni, R and Weinberger, J. Management of intracerebral hemorrhage. *Vascular Health and Risk Management*. 2007;3:701–709.
- [4] Hemphill, JC, Bonovich, DC, Besmertis, L, Manley, GT, and Johnston, SC. The ICH score a simple, reliable grading scale for intracerebral hemorrhage. *Stroke*. 2001;32:891–897.
- [5] Diringer, MN, Edwards, DF, and Zazulia, AR. Hydrocephalus: a previously unrecognized predictor of poor outcome from supratentorial intracerebral hemorrhage. *Stroke*. 1998;29:1352–1357.
- [6] Ariesen, MJ, Algra, A, Worp, HB Van der, and Rinkel, GJE. Applicability and relevance of models that predict short term outcome after intracerebral haemorrhage. *Journal of Neurology, Neurosurgery & Psychiatry*. 2005;76:839–844.
- [7] Selim, M, Fink, JN, Kumar, S, Caplan, LR, Horkan, C, Chen, Y, et al. Predictors of hemorrhagic transformation after intravenous recombinant tissue plasminogen activator prognostic value of the initial apparent diffusion coefficient and diffusion-weighted lesion volume. *Stroke*. 2002;33:2047–2052.
- [8] Hallevy, C, Ifergane, G, Kordysh, E, and Herishanu, Y. Spontaneous supratentorial intracerebral hemorrhage: criteria for short-term functional outcome prediction. *Journal of Neurology*. 2002;249:1704–1709.
- [9] Cheung, RTF and Zou, LY. Use of the original, modified, or new intracerebral hemorrhage score to predict mortality and morbidity after intracerebral hemorrhage. *Stroke*. 2003;34:1717–1722.
- [10] Mendelow, AD, Gregson, BA, Fernandes, HM, Murray, GD, Teasdale, GM, Hope, DT, et al. Early surgery versus initial conservative treatment in patients with spontaneous supratentorial intracerebral haematomas in the international surgical trial in intracerebral haemorrhage (STICH): a randomised trial. *The Lancet*. 2005;365:387–397.
- [11] Mendelow, AD, Gregson, BA, Rowan, EN, Murray, GD, Ghokal, A, and Mitchell, PM. Early surgery versus initial conservative treatment in patients with spontaneous supratentorial lobar intracerebral haematomas (STICH II): a randomised trial. *The Lancet*. 2013;382:397–408.

- [12] Anderson, CS, Huang, Y, Wang, JG, Arima, H, Neal, B, Peng, B, et al. Intensive blood pressure reduction in acute cerebral haemorrhage trial (INTERACT): a randomised pilot trial. *The Lancet Neurology*. 2008;7:391–399.
- [13] Acute Cerebral Hemorrhage (ATACH) investigators, AT of. Antihypertensive treatment of acute cerebral hemorrhage. *Critical Care Medicine February 2010*. 2010;38:637–648.
- [14] Menezes, NM, Ay, H, Zhu, MW, Lopez, CJ, Singhal, AB, Karonen, JO, et al. The real estate factor quantifying the impact of infarct location on stroke severity. *Stroke*. 2007;38:194–197.
- [15] Ziai, WC, Tuhrim, S, Lane, K, McBee, N, Lees, K, Dawson, J, et al. A multicenter, randomized, double-blinded, placebo-controlled phase III study of clot lysis evaluation of accelerated resolution of intraventricular hemorrhage (CLEAR III). *International Journal of Stroke*. 2014;9:536–542.
- [16] Rorden, C, Bonilha, L, Fridriksson, J, Bender, B, and Karnath, HO. Age-specific CT and MRI templates for spatial normalization. *NeuroImage*. 2012;61:957–965.
- [17] Solomon, J, Raymont, V, Braun, A, Butman, JA, and Grafman, J. User-friendly software for the analysis of brain lesions (ABLE). *Computer Methods and Programs in Biomedicine*. 2007;86:245–254.
- [18] Li, Y, Wu, J, Chen, Z, Jia, F, and Hu, Q. Registration of head CT images with subarachnoid hemorrhage. In: *Biomedical Engineering and Informatics (BMEI), 2010 3rd International Conference on*. IEEE. 2010;2:498–502.
- [19] Princich, JP, Wassermann, D, Latini, F, Oddo, S, Blenkmann, AO, Seifer, G, et al. Rapid and efficient localization of depth electrodes and cortical labeling using free and open source medical software in epilepsy surgery candidates. *Frontiers in Neuroscience*. 2013;7.
- [20] Brott, T, Adams, HP, Olinger, CP, Marler, JR, Barsan, WG, Biller, J, et al. Measurements of acute cerebral infarction: a clinical examination scale. *Stroke*. 1989;20:864–870.
- [21] Teasdale, G and Jennett, B. ASSESSMENT OF COMA AND IMPAIRED CONSCIOUSNESS: a practical scale. *The Lancet*. 1974;304:81–84.
- [22] Teasdale, G and Jennett, B. Assessment and prognosis of coma after head injury. *Acta Neurochirurgica*. 1976;34:45–55.
- [23] Mould, WA, Carhuapoma, JR, Muschelli, J, Lane, K, Morgan, TC, McBee, NA, et al. Minimally invasive surgery plus recombinant tissue-type plasminogen activator for intracerebral hemorrhage evacuation decreases perihematomal edema. *Stroke*. 2013;44:627–634.

- [24] Bergström, M, Ericson, K, Levander, B, Svendsen, P, and Larsson, S. Variation with time of the attenuation values of intracranial hematomas. *Journal of computer assisted tomography*. 1977;1:57–63.
- [25] Smith, EE, Rosand, J, and Greenberg, SM. Imaging of hemorrhagic stroke. *Magnetic Resonance Imaging Clinics of North America*. 2006;14:127–140.
- [26] Ashburner, J and Friston, KJ. Unified segmentation. *NeuroImage*. 2005;26:839–851.
- [27] Muschelli, J, Sweeney, E, and Crainiceanu, C. brainR: interactive 3 and 4d images of high resolution neuroimage data. *R Journal*. 2014;6:41–48.
- [28] Oishi, K, Zilles, K, Amunts, K, Faria, A, Jiang, H, Li, X, et al. Human brain white matter atlas: identification and assignment of common anatomical structures in superficial white matter. *NeuroImage*. 2008;43:447–457.
- [29] Akaike, H. Information theory and an extension of the maximum likelihood principle. In: *Second international symposium on information theory*. Akademinai Kiado. 1973. 267–281.
- [30] Venkatasubramanian, C, Kleinman, JT, Fischbein, NJ, Olivot, JM, Gean, AD, Eynporn, I, et al. Natural history and prognostic value of corticospinal tract wallerian degeneration in intracerebral hemorrhage. *Journal of the American Heart Association*. 2013;2:e000090.
- [31] Waller, A. Experiments on the section of the glossopharyngeal and hypoglossal nerves of the frog, and observations of the alterations produced thereby in the structure of their primitive fibres. *Philosophical Transactions of the Royal Society of London*. 1850;140:423–429.
- [32] Jang, SH, Ahn, SH, Sakong, J, Byun, WM, Choi, BY, Chang, CH, et al. Comparison of TMS and DTT for predicting motor outcome in intracerebral hemorrhage. *Journal of the Neurological Sciences*. 2010;290:107–111.
- [33] Demeurisse, G, Demol, O, and Robaye, E. Motor evaluation in vascular hemiplegia. *European neurology*. 1980;19:382–389.
- [34] Brunnstrom, S. Motor testing procedures in hemiplegia: based on sequential recovery stages. *Physical Therapy*. 1966;46:357.
- [35] Schaechter, JD, Fricker, ZP, Perdue, KL, Helmer, KG, Vangel, MG, Greve, DN, et al. Microstructural status of ipsilesional and contralesional corticospinal tract correlates with motor skill in chronic stroke patients. *Human Brain Mapping*. 2009;30:3461–3474.
- [36] Kumral, E, Kocaer, T, Ertbey, N, and Kumral, K. Thalamic hemorrhage a prospective study of 100 patients. *Stroke*. 1995;26:964–970.
- [37] Rankin, J. Cerebral vascular accidents in patients over the age of 60. II. prognosis. *Scottish medical journal*. 1957;2:200–215.

- [38] Swieten, JCv, Koudstaal, PJ, Visser, MC, Schouten, HJ, and Gijn, Jv. Interobserver agreement for the assessment of handicap in stroke patients. *Stroke*. 1988;19:604–607.
- [39] Eloyan, A, Shou, H, Shinohara, RT, Sweeney, EM, Nebel, MB, Cuzzocreo, JL, et al. Health effects of lesion localization in multiple sclerosis: spatial registration and confounding adjustment. *PloS one*. 2014;9:e107263.

Figure Legends

Figure 1. ICH engagement prevalence. The proportion of patients with ICH engaging a given voxel are represented in a 3D histogram (right side of image is left side of brain) overlaid on an MRI T1 template. There is a higher prevalence of ICH on the left side of the brain, localized in the middle of the brain, with few extensions in the anterior and posterior areas. The interactive version of this figure is located at http://muscchellij2.github.io/CT_Pipeline/index.html.

Figure 2. P-value maps for the voxel-wise NIHSS models. In the unadjusted (panel A) or sex-adjusted (not shown) linear models, voxels with the smallest p-values appear medial near the lateral ventricles. In age-adjusted (panel B), total baseline ICH volume-adjusted (not shown), or age and volume-adjusted (panel C), the p-values relating to NIHSS scores appear higher (more bluish). The Wilcoxon rank-sum test (D) have smaller p-values for the same area compared to the unadjusted linear model.

Figure 3. Highest Predictive Region (HPR) Analysis. Panels (A) and (B) correspond to the HPR for the top-performing model for NIHSS and GCS scores. The HPR in (A) represents a p-value threshold of .0100 (19047 voxels) for the voxel-wise p-value of ICH on NIHSS. The HPR in (B) represents 1000 with the lowest p-values for the voxel-wise ICH on GCS score regressions. Panels (C) and (D) plot the relationship of the HPR coverage ($HPR\ Coverage_i = \frac{\# \text{ Voxels classified ICH in HPR for scan } i}{\# \text{ Voxels in HPR}} \times 100\%$) and severity score. The red line represents a linear fit, the blue line—a LOESS fit. The larger the HPR coverage the higher (more severe) the NIHSS and the lower (deeper unconsciousness) the GCS.

Tables

Variable (N = 111)	N (%) or Mean (SD)
Age in Years: Mean (SD)	60.8 (11.2)
Sex: Female	35 (31.5%)
NIHSS Score: Mean (SD)	22.1 (8.7)
GCS Score: Mean (SD)	10.0 (3.0)
ICH Volume: Mean (SD)	37.4 (20.1)
IVH Volume: Mean (SD)	3.2 (6.3)
Race	
Caucasian not Hispanic	59 (53.2%)
African American not Hispanic	35 (31.5%)
Hispanic	12 (10.8%)
Asian or Pacific Islander	5 (4.5%)
Reader-Classified ICH Location	
Putamen	68 (61.3%)
Lobar	33 (29.7%)
Globus Pallidus	6 (5.4%)
Thalamus	4 (3.6%)

Table 1. Descriptive statistics of the demographic information for the patients.

Number of Voxels	P-value	Adjusted R^2	R^2	AIC	RMSE
NIHSS Score					
Location Model		0.129	0.178	18.60	8.116
1000	.0005	0.236	0.265	2.47	7.598
2000	.0009	0.234	0.263	2.81	7.610
2422	.0010	0.247	0.275	0.98	7.545
3000	.0013	0.244	0.272	1.46	7.562
19047	.0100	0.254	0.282	0.00	7.511
47736	.0500	0.248	0.276	0.77	7.538
GCS Score					
Location Model		0.069	0.120	20.51	2.914
1000	.0002	0.214	0.243	0.00	2.677
2000	.0004	0.213	0.242	0.09	2.678
3000	.0006	0.212	0.241	0.25	2.680
4669	.0010	0.212	0.241	0.23	2.680
22858	.0100	0.191	0.221	3.17	2.716
52368	.0500	0.166	0.197	6.44	2.757

Table 2. Table of model-fit measures for regression models using HPR coverage or reader-based location on GCS and NIHSS scores

Area	Population Prevalence	NIHSS HPR	GCS HPR
CSF	7.9	10.9	4.2
Insular	7.6		
Superior temporal gyrus	5.5		
Putamen	4.8	4.3	
External capsule	3.9		
Superior corona radiata	3.7	11.0	27.9
Precentral gyrus	3.3		
Precentral WM	3.1		1.3
Superior temporal WM	3.1		
Posterior limb of internal capsule	3.0	12.0	3.9
Thalamus		10.1	33.9
Caudate nucleus		8.4	9.6
Anterior limb of internal capsule		6.8	
Globus pallidus		6.0	
Superior longitudinal fasciculus		4.5	5.9
Outside brain mask		3.6	
Postcentral WM			6.7
Posterior corona radiata			3.1
Supramarginal WM			1.1

Table 3. Distribution of the top 10 areas of engagement

Figures

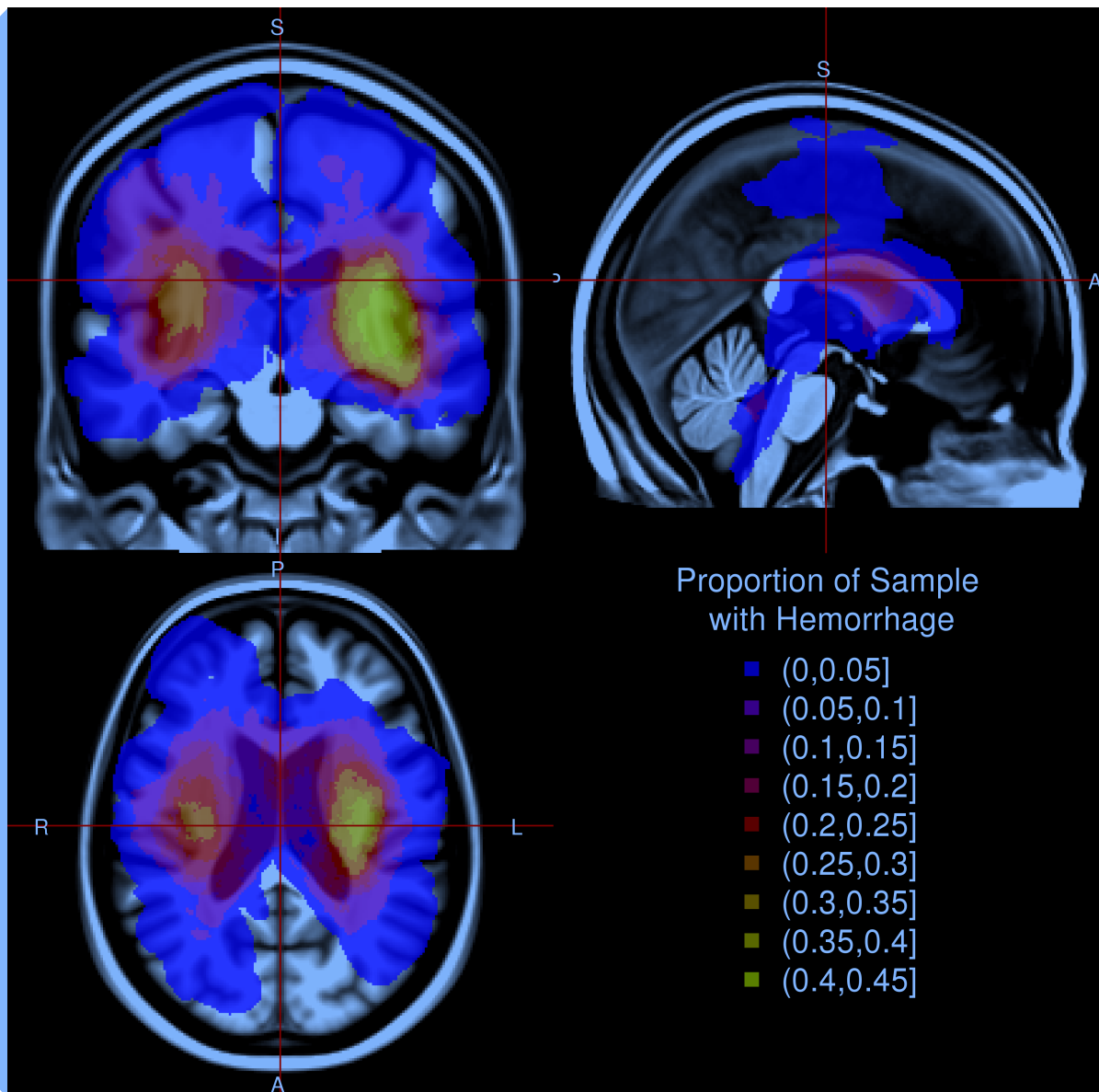


Figure 1

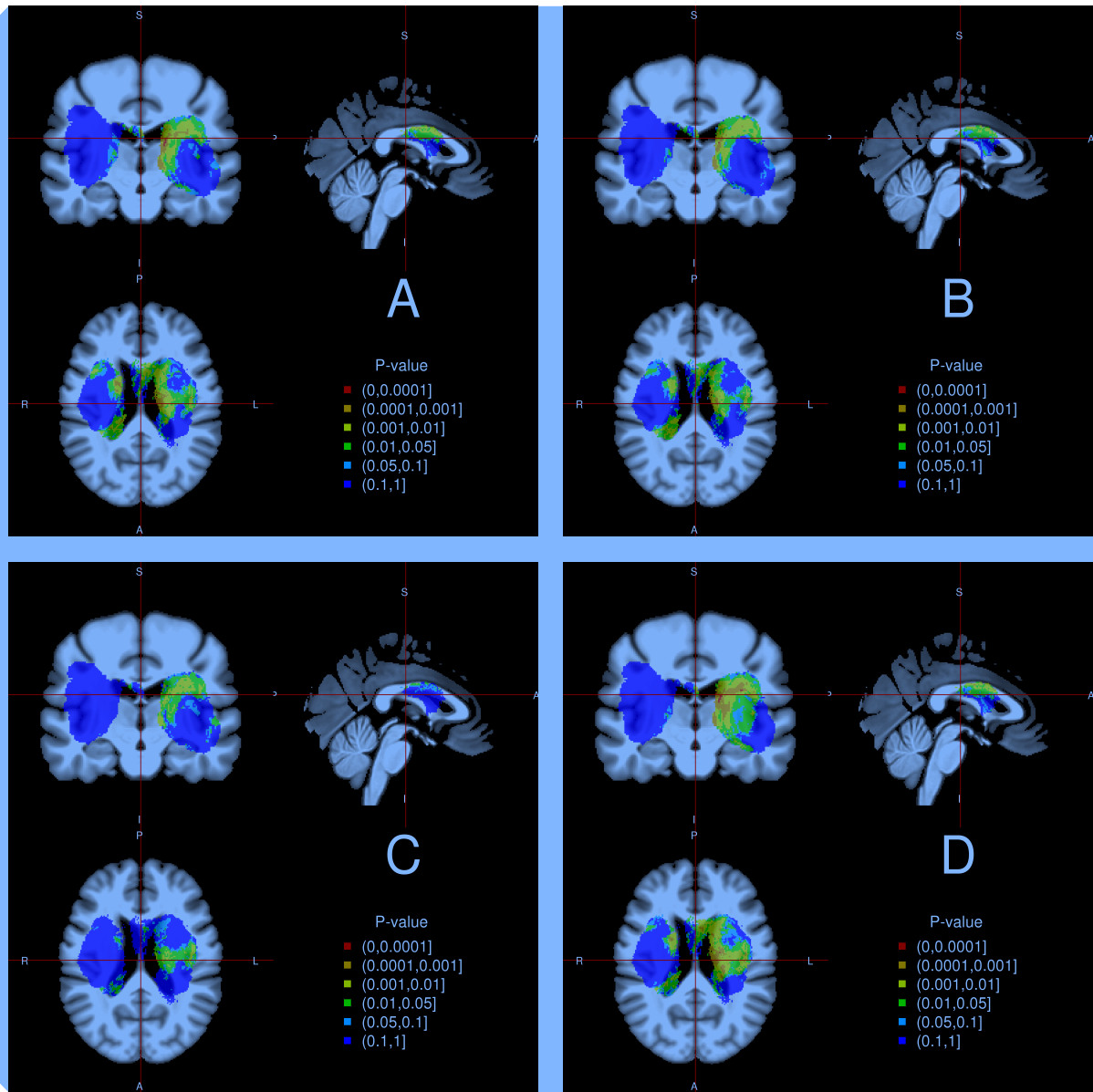


Figure 2

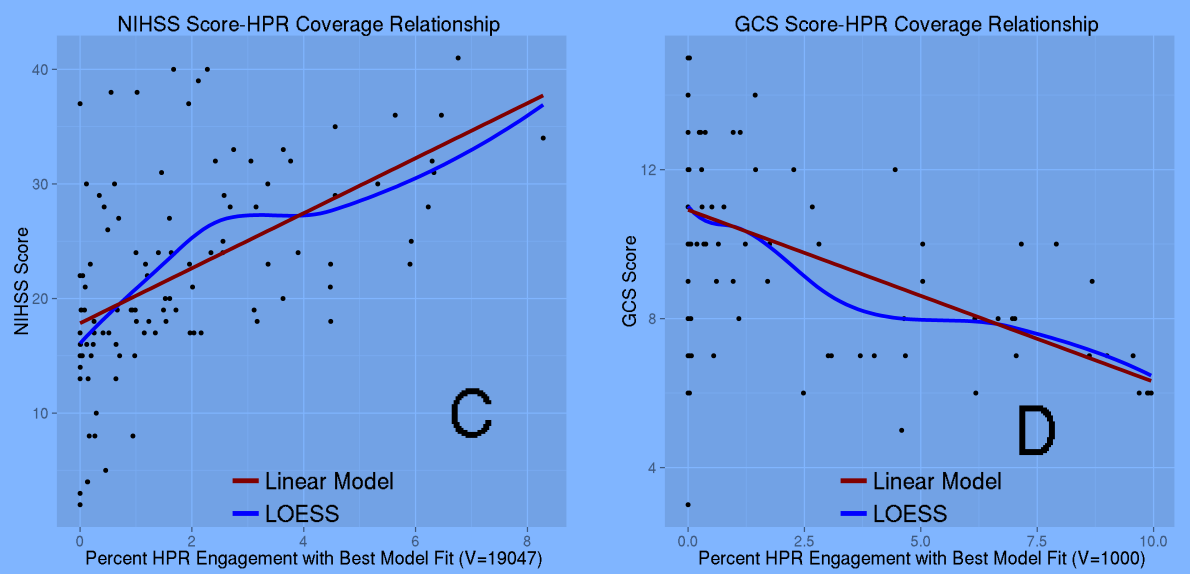
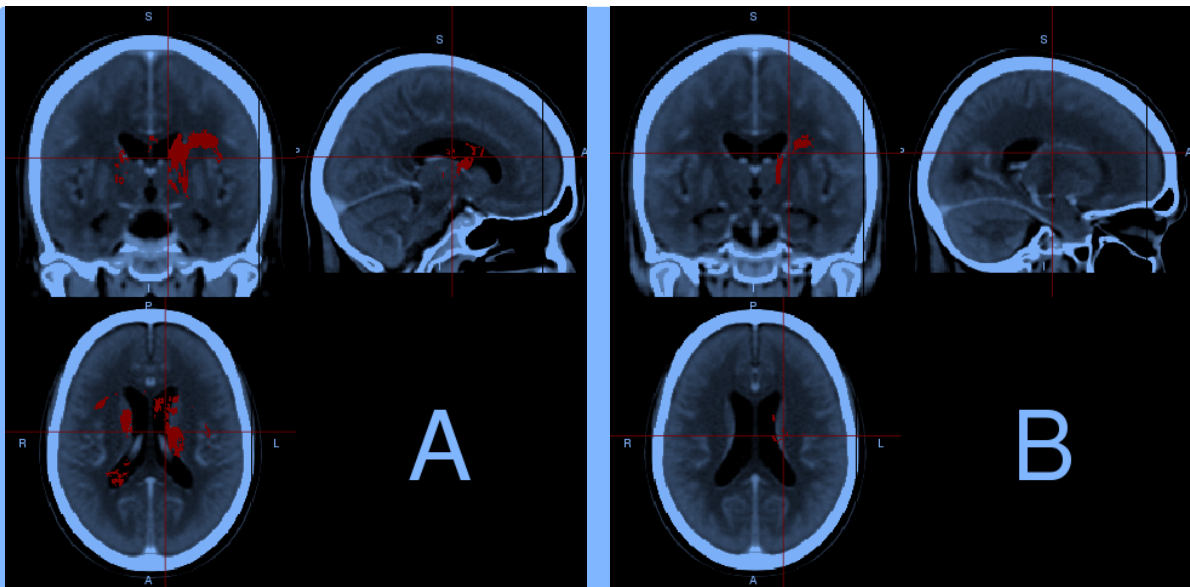


Figure 3

Supplemental Material

Supplemental Methods

Image Processing: Brain Extraction, Reorientation, Registration

The hemorrhage was excluded when registering the CT scan to the template using manual ICH segmentations. Binary ICH masks had voxel values of 1 if the voxel was hemorrhage, and 0 otherwise.

The CT images were processed as follows:

1. Export from OsiriX to DICOM format
2. Gantry tilt corrected (if applicable) using MATLAB script (<http://bit.ly/1ltIM8c>)
3. Converted to the Neuroimaging Informatics Technology Initiative (NIfTI) format using `dcm2nii` (2009 version, MRIcro [1])
4. Brain extraction tool (BET) [2], a function of FSL (v5.0.4) [3] was applied
5. The data was aligned to the anterior-posterior commissure line (<http://bit.ly/1gUqMDw>).
6. The Clinical MATLAB toolbox [4] transformed the image and mask into template space.

An image with its brain-extracted counterpart is displayed in Supplemental Figure IB.

We thresholded the registered-to-template hemorrhage mask: let S_i be the mask for person i , and s_{ij} be the intensity of voxel j of that mask; let v_{ij} represents voxel j of the thresholded image. The was thresholded using the rule [4]:

$$v_{ij} = \begin{cases} 1 & \text{if } s_{ij} \geq \frac{\min(S_i) + \max(S_i)}{2} \\ 0 & \text{if } s_{ij} < \frac{\min(S_i) + \max(S_i)}{2} \end{cases}$$

These binary ICH masks were used in analysis.

Calculating Region Engagement from the Eve Atlas

We also calculated the percent engagement of regions for the best-performing HPR for the NIHSS and GCS score analyses. More explicitly, let k denote the brain region (e.g. Putamen) and let $\sum_k v_k$ represent the sum of the voxels for an image (HPR or population ICH image) in that brain region. These p_k represent the percent that brain region engages the ICH compared to other regions (Table 3):

$$p_k = \frac{\sum_k v_k}{\text{Sum of Voxels in Analysis}}$$

We also calculated brain region engagement with the population ICH or HPR images (Table II):

$$r_k = \frac{\sum_k v_k}{\#\text{Number of Voxels in Region}}$$

These percentages (r_k) are at a region level; p_k are at an image level.

Image Registration

We present the registration results (Figure I): manually segmented blood in the original space with the hemorrhage mask in pink (panel A), brain-extracted image (panel B), registered image and hemorrhage mask in template space (panel C), and the ICH mask on the template (panel D). These images represent one patient with variable slice thickness with a large hemorrhage.

Though variable slice thickness is present, the transformation morphs the image into the full space of the template; therefore, non-linear registration seems to reasonably account for variable slice thickness, likely by non-uniform scaling. Gross brain features remain relatively unchanged, but large deformations of tissue, due to ICH, appear well preserved by registration.

Supplemental Tables

	NIHSS Score		GCS Score	
	HPR Coverage	Reader-Based	HPR Coverage	Reader-Based
Age	-0.04 (-0.2, 0.1)	-0.1 (-0.2, 0.1)	0.02 (-0.03, 0.1)	0.02 (-0.03, 0.1)
Sex: Male vs. Female	-0.7 (-3.8, 2.4)	-1.7 (-5.0, 1.7)	0.03 (-1.1, 1.1)	0.1 (-1.1, 1.3)
TICHVol per 10 cc	0.8 (-0.003, 1.5)	1.6 (0.8, 2.4)	-0.2 (-0.5, 0.02)	-0.5 (-0.7, -0.2)
HPR Coverage per 10%	2.0 (1.1, 2.8)		-0.4 (-0.6, -0.2)	
Reader-Based Location				
Globus Pallidus		4.5 (-2.9, 11.9)		-1.8 (-4.5, 0.8)
Putamen		4.2 (0.3, 8.2)		-1.2 (-2.6, 0.2)
Thalamus		4.8 (-4.1, 13.6)		-1.0 (-4.2, 2.1)
Constant	18.8 (9.1, 28.4)	19.6 (7.5, 31.7)	10.6 (7.4, 13.7)	11.2 (6.9, 15.5)

Table I. Severity Score Regression Models for HPR-Based and Reader-Classified Location

Area	Population Engagement	NIHSS HPR	GCS HPR
Globus Pallidus: Total	20.3	40.0	0.0
Globus Pallidus: Right	14.8	34.8	0.0
Globus Pallidus: Left	25.2	44.7	0.0
Putamen: Total	23.3	6.6	0.0
Putamen: Right	17.5	3.8	0.0
Putamen: Left	29.2	9.4	0.0
Thalamus: Total	7.9	8.9	1.7
Thalamus: Right	6.8	3.1	0.0
Thalamus: Left	9.1	14.6	3.4

Table II. Thalamus, Putamen and Globus Pallidus ICH Engagement by the population and NIHSS/GCS HPR

Supplemental Figures and Figure Legends

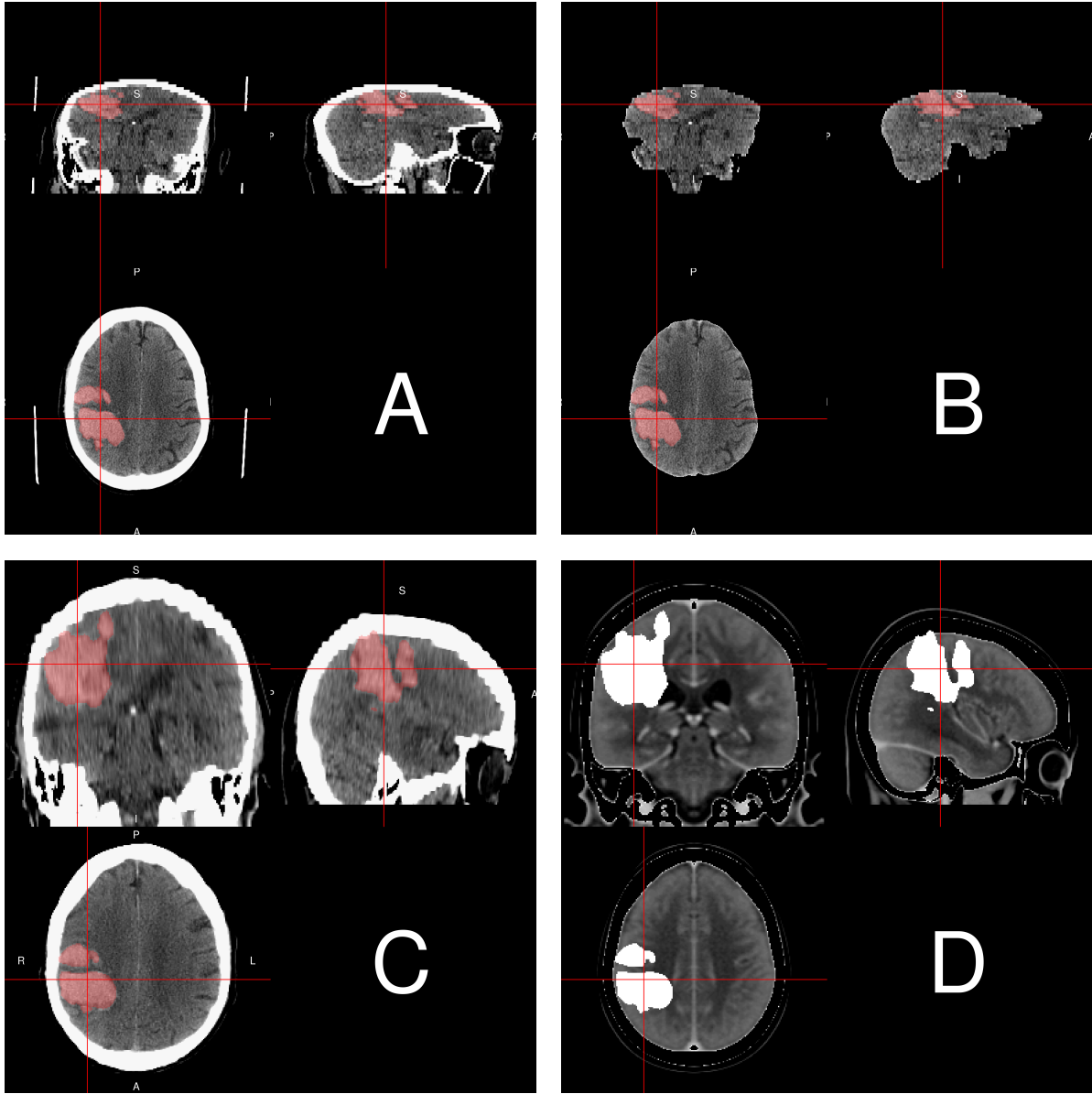


Figure I. Steps of Image Processing. The native space image (A), with hemorrhage overlaid (pink), shows variable slice thickness: the top of the brain has smaller voxel sizes than the bottom of the brain. The brain-extracted image used for AC-PC alignment is in panel (B). The template-registered image (C) was transformed and scaled to size as the template. We see that similar structures, such as the lateral ventricles, are observed on the same axial slice on the patient-level scan compared to the template image, which indicates adequate registration. Panel (D) shows the overlaid hemorrhage mask on the CT template.

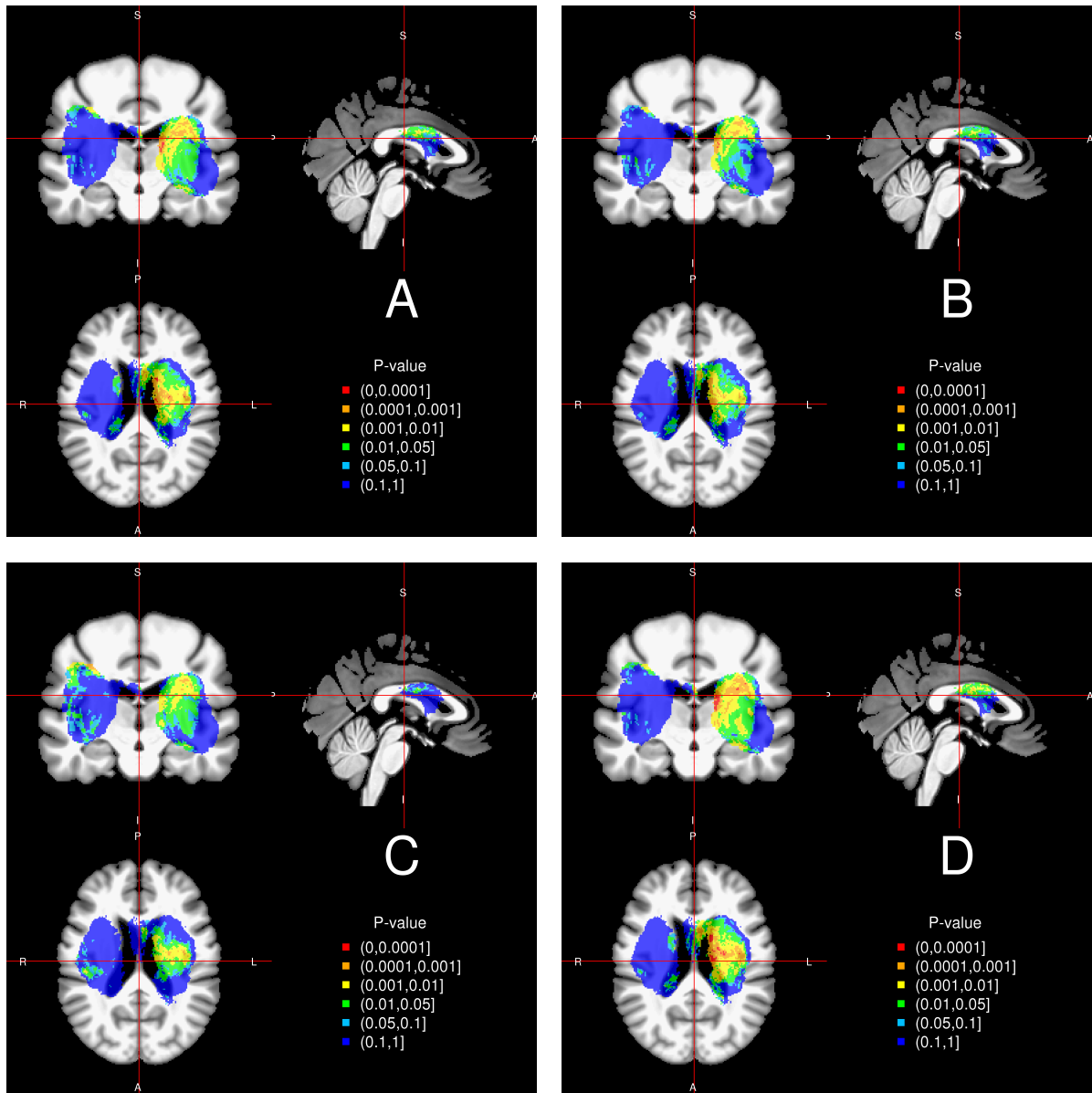


Figure II. P-value maps for the voxel-wise GCS models. In the unadjusted linear model (panel (A)) and after adjusting for sex (not shown, similar to (A)) there are voxels with the smallest p-values seem to be near the lateral ventricles. In models adjusting for age (B), or total baseline ICH volume (not shown, similar to (D)), or both (C), the p-value relating to GCS scores appear higher (more bluish). Also, we see the Wilcoxon rank-sum test has smaller p-values for the same area compared to the unadjusted linear model (D).

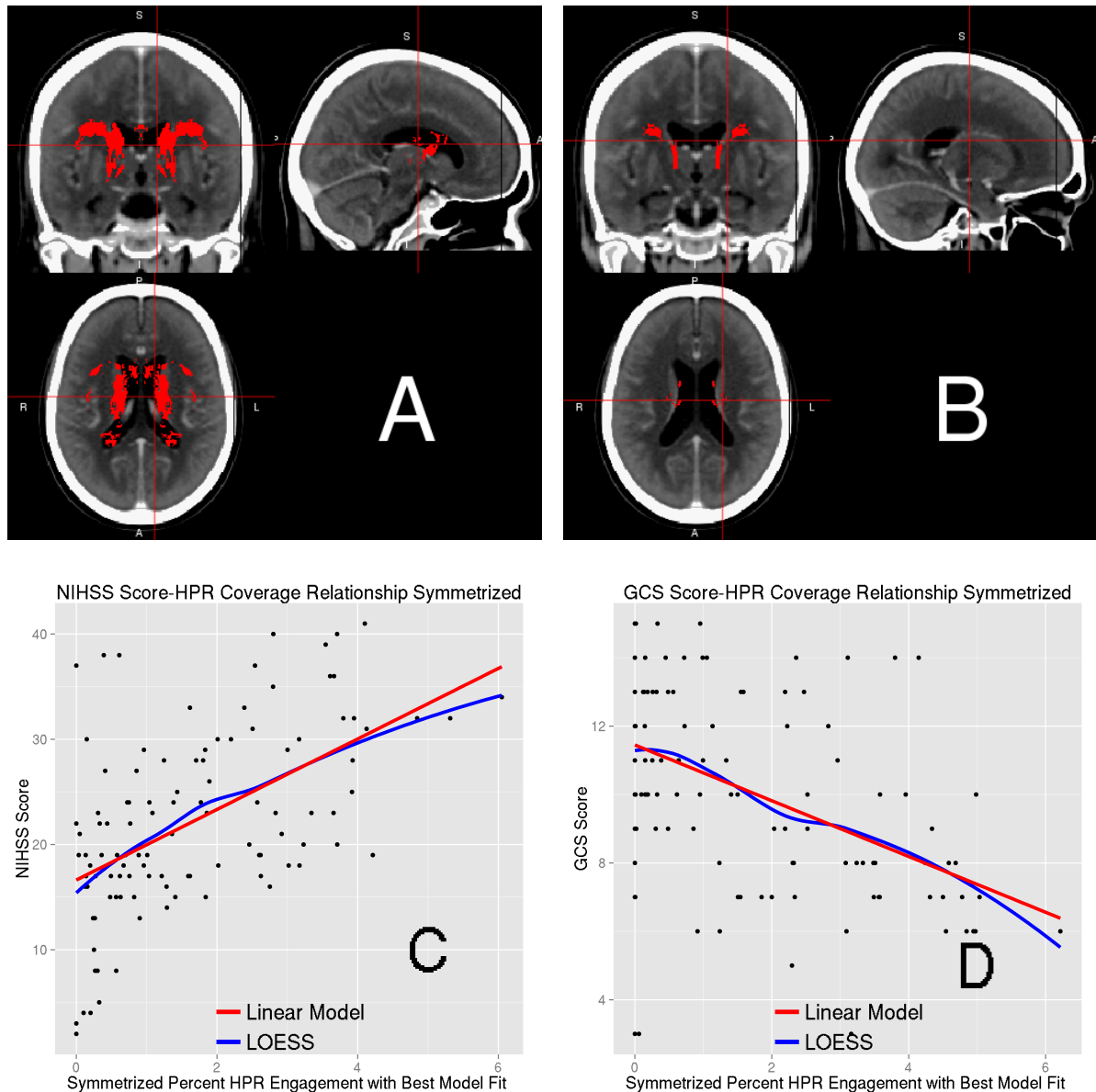


Figure III. Highest Predictive Region (HPR) Analysis with Symmetrized HPR. HPR were symmetrized by including voxels in the HPR and the voxel on the contra-lateral side. Panels (A) and (B) correspond to the symmetrized HPR for NIHSS (Figure 3(A)) and GCS (Figure 3(B)), respectively. Panels (C) and (D) plot the symmetrized HPR coverage-severity score relationship. The larger the HPR coverage the higher (more severe stroke) the NIHSS score and the lower (deeper unconsciousness) the GCS score.

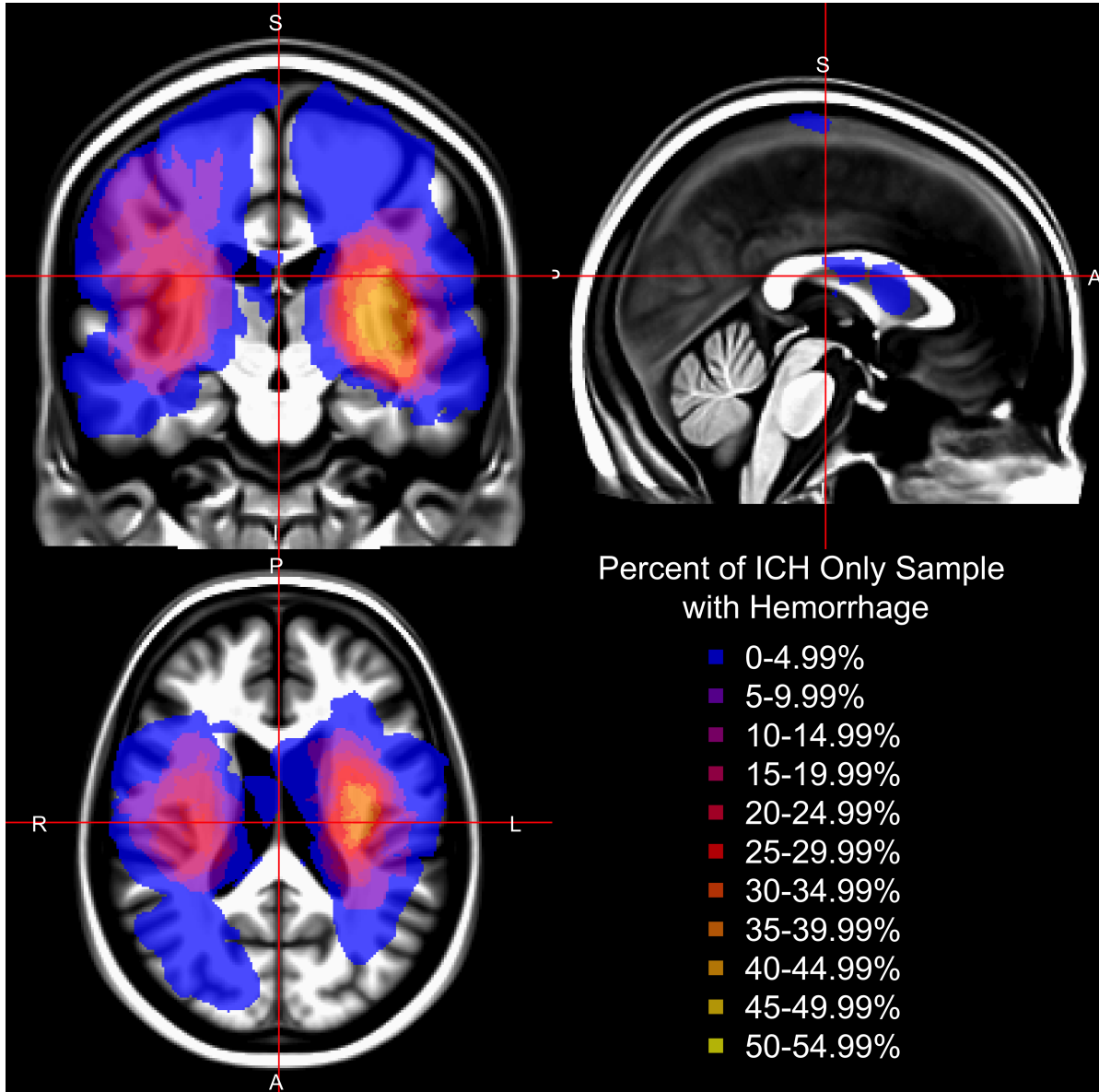


Figure IV. ICH engagement prevalence in patients with no recorded IVH.
The proportion of patients with ICH, but without IVH, engaging a given voxel are represented in a 3D histogram (right side of image is left side of brain) overlaid on an MRI T1 template. Note that areas of the ventricles have a low prevalence (indicated by blue), indicating that much of the prevalence in the ventricular spaces the full population of images is due to IVH.

Supplemental References

- [1] Rorden, C and Brett, M. Stereotaxic display of brain lesions. *Behavioural Neurology*. 2000;12:191–200.
- [2] Smith, SM. Fast robust automated brain extraction. *Human Brain Mapping*. 2002;17:143–155.
- [3] Jenkinson, M, Beckmann, CF, Behrens, TEJ, Woolrich, MW, and Smith, SM. FSL. *NeuroImage*. 2012;62:782–790.
- [4] Rorden, C, Bonilha, L, Fridriksson, J, Bender, B, and Karnath, HO. Age-specific CT and MRI templates for spatial normalization. *NeuroImage*. 2012;61:957–965.